Vertex-corrected perturbation theory for the electron-phonon problem with nonconstant density of states

J. K. Freericks
Department of Physics, Georgetown University, Washington, D.C. 20057

V. Zlatić
Institute of Physics, 10000 Zagreb, Croatia

Woonki Chung
Department of Physics, Georgetown University, Washington, D.C. 20057

Mark Jarrell
Department of Physics, University of Cincinnati, Cincinnati, Ohio 45221

(Received 23 June 1998)

A series of weak-coupling perturbation theories that include the lowest-order vertex corrections are applied to the attractive Holstein model in infinite dimensions. The approximations are chosen to reproduce the iterated perturbation theory in the limit of half-filling and large phonon frequency (where the Holstein model maps onto the Hubbard model). Comparison is made with quantum Monte Carlo solutions to test the accuracy of different approximation schemes. [S0163-1829(98)02541-7]

I. INTRODUCTION

The theory of superconductivity, as first developed by Bardeen, Cooper, and Schrieffer,[1] and then generalized to strong coupling by Migdal,[2] Eliashberg,[3] and others,[4,5] has proven to be one of the most accurate theories of solid-state physics. Properties of conventional low-T_c materials are typically explained to accuracies of 1% or better. Newly discovered materials, however, which have moderate T_c's, do not fit into the parameter regimes studied so successfully in the 1950s and 1960s. These materials, such as the $A15$ compounds, $Ba_{1-x}K_xBiO_3$, and K_3C_{60} have large phonon energy scales relative to the inverse electronic density of states, so that both the effect of the energy dependence of the bare electronic density of states (i.e., nonconstant density of states), and the effect of vertex corrections may become important in their description. We examine here a series of different weak-coupling perturbation theories that include both the effects of nonconstant density of states and of vertex corrections to ascertain what methods should be used for real materials calculations of these higher T_c compounds. Since the most popular implementation of Migdal-Eliashberg theory is manifestly particle-hole symmetric (because of the neglect of the energy dependence of the electronic density of states) it is not clear what the most accurate approximation scheme is when the electron filling is doped away from half filling and the energy dependence of the electronic density of states becomes important. Our strategy is to solve a model system (the Holstein model) in the infinite-dimensional limit via the dynamical mean-field theory. This allows us to compare numerically exact quantum Monte Carlo solutions (in the thermodynamic limit) with the different perturbative approximations.

The Holstein model[6] consists of conduction electrons that interact with local (Einstein) phonons:

$$H=-\frac{t^*}{2\sqrt{d}}\sum_{\langle j,k\rangle\sigma}(c^\dagger_{j\sigma}c_{k\sigma}+c^\dagger_{k\sigma}c_{j\sigma})+\sum_j (gx_j-\mu)(n_{j\uparrow}+n_{j\downarrow})+\frac{1}{2}M\Omega^2\sum_j x_j^2+\frac{1}{2}\sum_j \frac{p_j^2}{M}. \quad (1)$$

In Eq. (1), $c^\dagger_{j\sigma}$ ($c_{j\sigma}$) creates (destroys) an electron at site j with spin σ, $n_{j\sigma}=c^\dagger_{j\sigma}c_{j\sigma}$ is the electron number operator, and x_j (p_j) is the phonon coordinate (momentum) at site j. The hopping is chosen to be between the nearest neighbors (j and k) of a hypercubic lattice in d dimensions and the unit of energy is the rescaled matrix element t^* (so that the kinetic energy remains finite as $d\to\infty$). The phonon has a mass M (chosen to be $M=1$), a frequency Ω, and a spring constant $\kappa\equiv M\Omega^2$ associated with it. The deformation potential is denoted by g and it governs the strength of the coupling of electrons to phonons. The effective electron-electron interaction strength (mediated by the phonons) is then the bipolaron binding energy

$$U\equiv-\frac{g^2}{M\Omega^2}=-\frac{g^2}{\kappa}. \quad (2)$$

A chemical potential μ is employed to adjust the total electron filling with $\mu=U$ corresponding to half filling in the exact solution.

In the instantaneous limit where U remains finite and g and Ω are large compared to the bandwidth ($g,\Omega\to\infty$, U = finite), the Holstein model maps onto the attractive Hubbard model[7]

$$H=-\frac{t^*}{2\sqrt{d}}\sum_{\langle j,k\rangle\sigma}(c^\dagger_{j\sigma}c_{k\sigma}+c^\dagger_{k\sigma}c_{j\sigma})$$
$$-\left(\mu-\frac{U}{2}\right)\sum_j(n_{j\uparrow}+n_{j\downarrow})+U\sum_j n_{j\uparrow}n_{j\downarrow}, \qquad (3)$$

with U defined by Eq. (2).

Two cases of the Holstein Hamiltonian have well-established perturbative expansions. In the limit where the phonon frequency becomes small $\Omega\to 0$, but U remains finite, Migdal-Eliashberg theory[2,3] is known to be an accurate approximation. Migdal-Eliashberg theory is a self-consistent Hartree-Fock approximation that employs fully dressed phonon propagators and neglects all vertex corrections. Typically, the energy dependence of the electronic density of states is also neglected, so the theory is evaluated with a constant density of states. (This latter approximation is always particle-hole symmetric and maps onto the limit of half filling when the nonconstant density of states is used.) The second limit is the large phonon frequency limit $\Omega\to\infty$ with U also remaining finite. In this case, a truncated perturbative expansion through second order[8,9] (which includes the lowest-order vertex correction) is known to be accurate at half filling for a large range of U values because it properly reproduces both the weak-coupling and strong-coupling limits of the Hubbard model. It would be nice to construct an approximation scheme that continuously connects these two limits as the phonon frequency is varied. However, no simple approximation can be found because the set of diagrams that dress the phonon propagator in the small-Ω limit do not correctly dress the phonon propagator in the large-Ω limit; in the large-frequency limit the interaction is only between up and down spins, but in the small-frequency limit the interaction is between all spins. But, if one is willing to examine perturbative expansions that are truncated with respect to the fluctuating diagrams, then approximations can be constructed that agree with the two known limits through the order of diagrams included in the expansion. The description of these different methods is both subtle and technical, and will be covered in detail in Sec. II. Here we only want to comment that the previous calculations for the electron-phonon problem that were called the iterated perturbation theory[9] (IPT) are actually based on a truncated perturbation theory about the Hartree mean-field theory solution, which does not reproduce the Migdal-Eliashberg (Hartree-Fock) limit properly. A more promising approach for all Ω is to construct a truncated perturbation theory about the Hartree-Fock mean-field theory solution, which is done here. In addition, we also examine some simple methods that can be used to repair inconsistencies that develop in the IPT as the system is doped off of half filling. This method entails self-consistently renormalizing the higher-order fluctuations of the Hartree or Fock diagrams to all orders, which allows for the electron filling on the lattice to be different from the electron filling of the mean-field theory solution when the higher-order fluctuations are included. Unfortunately, we find that all attempts to produce an accurate perturbation theory that reproduces the IPT in the instantaneous limit are not very accurate for moderate phonon frequencies.

These perturbative approaches, and the many-body problem in general, simplify when the infinite-dimensional limit[10] is taken ($d\to\infty$). Then the many-body problem becomes a local problem that retains its complicated dynamics in time. The hopping integral is scaled to zero in such a fashion that the free-electron kinetic energy remains finite while the self-energy for the single-particle Green's function and the irreducible vertex functions has no momentum dependence and is a functional of the local Green's function.[10–12] This limit retains the strong-correlation effects that arise from trying to simultaneously minimize both the kinetic energy and the potential energy, and hence has relevance for three-dimensional materials.

Of course, we can also solve the infinite-dimensional Holstein model using a quantum Monte Carlo (QMC) method, which contains all effects due to phonon renormalizations, vertex corrections, and nonconstant electronic density of states. We use these solutions as a benchmark to test the accuracy of the different approximation methods and to determine what is the most fruitful approximation for the electron-phonon problem.

We employ a Green's function formalism to solve the many-body problem. The local Green's function is defined to be

$$G_{loc}(i\omega_n)\equiv-\int_0^\beta d\tau e^{i\omega_n\tau}\frac{\mathrm{Tr}\langle e^{-\beta H}T_\tau c(\tau)c^\dagger(0)\rangle}{\mathrm{Tr}\langle e^{-\beta H}\rangle}, \qquad (4)$$

and is calculated directly from a self-consistent quantum Monte Carlo procedure described elsewhere.[13] Static two-particle properties can also be determined since the irreducible vertex function is local.[14] The static susceptibility for charge-density-wave (CDW) order is given by

$$\chi^{CDW}(\mathbf{q})=\frac{1}{2N}\sum_{\mathbf{R}_j-\mathbf{R}_k\sigma\sigma'}e^{i\mathbf{q}\cdot(\mathbf{R}_j-\mathbf{R}_k)}T\int_0^\beta d\tau$$
$$\times\int_0^\beta d\tau'[\langle n_{j\sigma}(\tau)n_{k\sigma'}(\tau')\rangle-\langle n_{j\sigma}(\tau)\rangle$$
$$\times\langle n_{k\sigma'}(\tau')\rangle]$$
$$=T\sum_{mn}\tilde{\chi}^{CDW}_{mn}(\mathbf{q}), \qquad (5)$$

at each ordering wave vector $\mathbf{q}$ [the indices m and n denote Matsubara frequencies $i\omega_n=i\pi T(2n+1)$]. Dyson's equation for the two-particle Green's function becomes[13,14]

$$\tilde{\chi}^{CDW}_{mn}(\mathbf{q})=\tilde{\chi}^0_m(\mathbf{q})\delta_{mn}-T\sum_p\tilde{\chi}^0_m(\mathbf{q})\Gamma^{CDW}_{mp}\tilde{\chi}^{CDW}_{pn}(\mathbf{q}), \qquad (6)$$

with Γ^{CDW}_{mn} the irreducible vertex function in the CDW channel.

The bare CDW susceptibility $\tilde{\chi}^0_n(\mathbf{q})$ in Eq. (6) is defined in terms of the *dressed* single-particle Green's function

$$\tilde{\chi}_n^0(\mathbf{q}) \equiv -\frac{1}{N}\sum_{\mathbf{k}} G_n(\mathbf{k})G_n(\mathbf{k}+\mathbf{q})$$
$$= -\frac{1}{\pi}\int_{-\infty}^{\infty} dy \frac{e^{-y^2}}{i\omega_n+\mu-\Sigma_n-y} \times \int_{-\infty}^{\infty} dz \frac{e^{-z^2}}{i\omega_n+\mu-\Sigma_n-X(\mathbf{q})y-z\sqrt{1-X^2(\mathbf{q})}} \tag{7}$$

with all of the wave-vector dependence described by the scalar[15,16] $X(\mathbf{q}) \equiv \Sigma_{j=1}^{d} \cos \mathbf{q}_j / d$. The integral for $\tilde{\chi}_m^0(X)$ in Eq. (7) can then be performed analytically[15] for the ''checkerboard'' CDW phase $\tilde{\chi}_n^0(X=-1) = -G_n/(i\omega_n+\mu-\Sigma_n)$. The irreducible vertex function Γ_{mn}^{CDW} is either directly calculated in a perturbative expansion (described below) or is determined by inverting the Dyson equation in Eq. (6) for the local charge susceptibility (QMC).

A similar procedure is used for the singlet s-wave superconducting (SC) channel. The corresponding definitions are as follows. The static susceptibility in the superconducting channel is defined to be

$$\chi^{SC}(\mathbf{q}) \equiv \frac{1}{N}\sum_{\mathbf{R}_j-\mathbf{R}_k} e^{i\mathbf{q}\cdot(\mathbf{R}_j-\mathbf{R}_k)} T \times \int_0^{\beta} d\tau \int_0^{\beta} d\tau' \langle c_{j\uparrow}(\tau) c_{j\downarrow}(\tau) c_{k\downarrow}^{\dagger}(\tau') c_{k\uparrow}^{\dagger}(\tau') \rangle$$
$$= T\sum_{mn} \tilde{\chi}_{mn}^{SC}(\mathbf{q}), \tag{8}$$

for superconducting pairs that carry momentum $\mathbf{q}$; Dyson's equation becomes

$$\tilde{\chi}_{mn}^{SC}(\mathbf{q}) = \tilde{\chi}_m^{0\prime}(\mathbf{q})\delta_{mn} - T\sum_{p} \tilde{\chi}_m^{0\prime}(\mathbf{q})\Gamma_{mp}^{SC}\tilde{\chi}_{pn}^{SC}(\mathbf{q}), \tag{9}$$

with Γ_{mn}^{SC} the corresponding irreducible vertex function to describe the SC channel; the bare pair-field susceptibility becomes

$$\tilde{\chi}_n^{0\prime}(\mathbf{q}) \equiv \frac{1}{N}\sum_{\mathbf{k}} G_n(\mathbf{k})G_{-n-1}(-\mathbf{k}+\mathbf{q})$$
$$= \frac{1}{\pi}\int_{-\infty}^{\infty} dy \frac{e^{-y^2}}{i\omega_n+\mu-\Sigma_n-y}\int_{-\infty}^{\infty} dz \times \frac{e^{-z^2}}{i\omega_{-n-1}+\mu-\Sigma_{-n-1}-X(\mathbf{q})y-z\sqrt{1-X^2(\mathbf{q})}} \tag{10}$$

with the special value $\tilde{\chi}_n^{0\prime}(X=1) = -\mathrm{Im}\, G_n/\mathrm{Im}(i\omega_n-\Sigma_n)$ for the SC pair that carries no net momentum; and finally the irreducible vertex function is also either directly calculated in a perturbative expansion (described below) or is determined by inverting the Dyson equation in Eq. (9) for the local pair-field susceptibility (QMC).

The transition temperature of the infinite-dimensional Holstein model is then found by calculating the temperature at which the relevant susceptibility diverges (CDW or SC). This transition temperature is found by locating the temperature where the scattering matrix (in the relevant channel)

$$T_{mn} = -T\Gamma_{mn}\tilde{\chi}_n^0 \tag{11}$$

has unit eigenvalue[17] (note that the local Green's functions are always used in the evaluation of the bare susceptibility $\tilde{\chi}_0$).

The remainder of the paper is arranged as follows: In Sec. II we describe the formalism employed to derive the different truncated perturbative expansions for both the electronic self-energy and for the irreducible vertex functions. Particular attention is paid to the mapping from the lattice problem onto an effective impurity problem, and how to extract a perturbative expansion that includes the lowest-order fluctuations beyond a mean-field theory solution. In Sec. III we describe the details of the calculational procedure and present our results in Sec. IV. Section V contains a summary and our conclusions.

II. LATTICE-IMPURITY MAPPING

The properties of the Holstein model are calculated by mapping the lattice problem onto the single-impurity Wolff-Holstein model[18,6] and solving the impurity self-energy by a truncated perturbation expansion. To define the mapping, we begin with the self-energy of the Holstein model, which is momentum independent in infinite dimensions, and write the local Green's function for the lattice as

$$G_{loc}(\omega) = \sum_{\mathbf{p}} \frac{1}{\omega-(\epsilon_{\mathbf{p}}-\mu)-\Sigma(\omega)}, \tag{12}$$

where $\epsilon_{\mathbf{p}}$ is the noninteracting electronic band structure for the lattice (assuming spin degeneracy $n_\uparrow = n_\downarrow = n/2$). The local self-energy $\Sigma(\omega)$ is defined by the functional, $\Sigma(\omega) = \Sigma[G_{loc}]$, where $\Sigma[G_{loc}]$ represents the sum of all the skeleton diagrams generated by the perturbation theory, with U as the expansion parameter (in a Baym-Kadanoff expansion[19]). On the other hand, the same set of skeleton diagrams appears in the self-energy of an impurity problem described by the Wolff-Holstein Hamiltonian,

$$H_{imp} = H_0 + g x_0 (n_{0\uparrow}+n_{0\downarrow}) + \frac{p_0^2}{2M} + \frac{1}{2}M\Omega^2 x_0^2, \tag{13}$$

where H_0 describes a band of noninteracting electrons, $n_{0\sigma}$ is the number operator for conduction electrons of spin σ at the impurity site, and x_0 (p_0) is the ''impurity'' phonon coordinate (momentum). The renormalized electron propagator at the impurity site can be written as

$$G_{imp}(\omega) = \frac{1}{G_0^{-1}(\omega)-\Sigma(\omega)}. \tag{14}$$

Here G_0 is the free-electron propagator at the impurity site (which is often called the effective-medium propagator), and $\Sigma(\omega)$ describes the effects due to the coupling to the local

phonon. Note that the effective medium G_0 is not equal to the noninteracting lattice propagator except when $U=0$.

Since the impurity and the lattice self-energy functionals $\Sigma[G_{imp}]$ and $\Sigma[G_{loc}]$ are the same, the self-energies will also be the same if $G_{imp}(\omega)=G_{loc}(\omega)$. Thus, the lattice problem maps onto the impurity problem, provided the effective medium propagator G_0 is adjusted so that the right-hand sides of Eqs. (12) and (14) are equal. In general, the self-energy functional $\Sigma[G_{loc}]$ is not known. But equivalent expansions can also be made for the impurity self-energy by rearranging the skeleton-diagram expansion. For example, a functional defined on the effective-medium propagator $G_0(\omega)$ can be employed, such that $\Sigma(\omega)=\Sigma_0[G_0]$, where $\Sigma_0[G_0]$ represents the sum of all connected graphs generated by Wick's theorem (without any resummations). If the graphs for $\Sigma[G_{loc}]$ and $\Sigma_0[G_0]$ are summed to all orders, then the self-energies must agree. Furthermore, the effective medium $G_0(\omega)$ can be uniquely determined by either $G_0^{-1}(\omega)=G_{loc}^{-1}(\omega)+\Sigma[G]$ or $G_0^{-1}(\omega)=G_{loc}^{-1}(\omega)+\Sigma_0[G_0]$.

Since the exact self-energy for the Wolff-Holstein model with an arbitrary density of states is not known, our strategy is to make a truncated expansion for the impurity self-energy functional $\Sigma_{app}[G_0]$, and define the self-energy for the lattice problem via $\Sigma(\omega)=\Sigma_{app}[G_0]$. The self-consistency is then imposed on $G_0(\omega)$, so that $G_{loc}(\omega)=G_{imp}(\omega)$. The hope is that a controlled expansion of the impurity self-energy will lead to an accurate solution of the impurity problem and of the resultant lattice problem. Here we use the lowest-order Yosida-Yamada expansion, which is known to provide reliable answers for the Wolff model describing magnetic impurities.[20,21]

The Yosida-Yamada expansion for the effective impurity problem (with an unknown density of states) is obtained by a partial resummation of diagrams that allows us to construct the self-energy functional in terms of diagrams that involve either Hartree or Hartree-Fock Green's functions. That is, one considers the self-energy corrections with respect to the mean-field solution, and rewrites the Dyson equation as

$$G_{imp}(\omega)=\frac{1}{[G_{MF}(\omega)]^{-1}-\Sigma_{YY}^{MF}[G_{MF}]}, \tag{15}$$

where Σ_{YY}^{MF} is the sum of all self-energy diagrams defined in terms of the mean-field propagator for the impurity problem G_{MF} and

$$G_{MF}^{-1}(\omega)=G_0^{-1}(\omega)-\Sigma_{MF}(\omega). \tag{16}$$

It is clear that functionals $\Sigma_{YY}^{MF}[G_{MF}]$ defined with different mean-field propagators are not the same, and it is not known *a priori* which truncated approximation for the impurity self-energy leads to the most accurate result for the lattice problem. The mean-field solution has an average electron filling n_{MF} defined by

$$n_{MF}=-\frac{2}{\pi}\,\mathrm{Im}\int d\omega G_{MF}(\omega)f(\omega) \tag{17}$$

with $f(w)=1/[1+\exp(\beta\omega)]$ the Fermi factor (the factor of 2 is from the spin summation). This filling is usually different from the electron filling on the lattice that is determined by the same equation, but with G_{MF} replaced by G_{loc}. In this contribution, we consider four different expansions to the self-energy and compare the corresponding results to the quantum Monte Carlo solution.

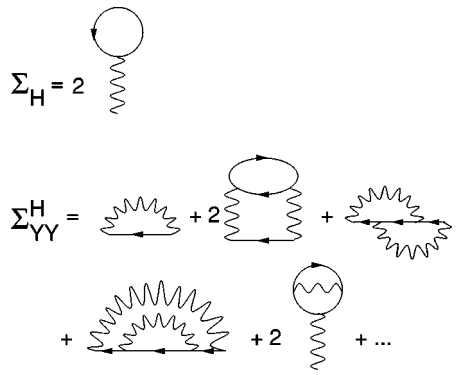

FIG. 1. Feynman diagrams included in the Hartree expansion. The top figure shows the Hartree diagram, which is incorporated into G_{MF}, and the bottom shows the Yosida-Yamada functional about the Hartree mean-field solution expanded through second order. The wiggly lines are bare phonon propagators and the straight lines are Hartree (mean-field) propagators. The fifth diagram that involves the Fock dressing of the Hartree diagram was not included in the previous work.

Our first approximation is called the Hartree expansion (H) and it includes a truncated perturbation-theory expansion about the Hartree mean-field solution, including all diagrams through second order. This expansion should not be confused with the Hartree approximation, which does not include any of the second-order vertex corrections. These self-energy corrections with respect to the Hartree mean-field solution are constructed by using the Hartree self-energy diagram shown in Fig. 1, to construct the mean-field propagator of Eq. (15). That is, we take

$$\Sigma_{MF}=\Sigma_H=Un_H, \tag{18}$$

which implies that the Hartree self-energy insertions are included to all orders in the perturbative expansion. Here n_H is the (Hartree) mean-field particle number defined by Eq. (17) with $G_{MF}=G_H$. Next, the Hartree mean-field Green's function is used in evaluating the truncated Yosida-Yamada self-energy functional to determine the approximate self-energy. This functional is given in Fig. 1 through second order in U where the electronic propagators (solid lines) are the Hartree mean-field propagators from Eq. (16), the phonon propagators (wiggly lines) are bare $D(\omega)=-1/[M(\Omega^2-\omega^2)]$, and the impurity self-energy that renormalizes the effective field G_0 in Eq. (14) becomes

$$\Sigma(\omega)=\Sigma_H+\Sigma_{YY}^H[G_H]. \tag{19}$$

Note that this procedure is summing an infinite class of diagrams (the Hartree self-energy insertions), but is truncating the perturbation theory *with respect to the Hartree mean-field theory solution* to include both the Fock and the second-order fluctuating terms. It turns out that this procedure is identical in form to what was previously called the IPT approximation,[9] since the renormalization of the effective medium by the Hartree self-energy (to construct the Hartree mean-field Green's function) can be absorbed by a redefini-

tion of the chemical potential (since the Hartree self-energy just provides a frequency-independent shift), with the exception being the inclusion of the fifth diagram, which renormalizes the Hartree diagram by the Fock self-energy insertion. The omission of the fifth diagram in the older IPT paper[9] may be thought to be innocuous because that diagram vanishes at half filling and should not greatly affect the results off of half filling. However, when the coupling strength becomes large, its effects do become strong, as shown in the next section. To reiterate, the difference between the present expansion and the older IPT work is that the fluctuating diagrams in $\Sigma_{YY}^{H}[G_H]$ are evaluated with G_H which does not include the frequency-independent shift from the fifth diagram of Fig. 1. The IPT calculation included the frequency-independent shifts to all orders, and hence evaluated the first four diagrams of Fig. 1 using a different mean-field propagator than G_H. The inclusion of the Fock self-energy insertion into the Hartree diagram is just one of the subtle, and often neglected, diagrams that needs to be included in a truncated approximation that includes all diagrams up to a given order.

Our second approximation is called the Hartree-Fock (HF) expansion and is obtained by using the Hartree-Fock self-energy

$$\Sigma_{MF}=\Sigma_{HF}=Un_{HF}+\Sigma_F \tag{20}$$

to define the mean-field propagator in Eq. (16) and including all second-order diagrams with respect to the Hartree-Fock mean-field solution (once again, this should not be confused with the Hartree-Fock approximation that does not include any of the second-order vertex corrections). The (Hartree-Fock) mean-field particle number n_{HF} is calculated by using G_{HF} in Eq. (17) and the Fock self-energy Σ_F satisfies

$$\Sigma_F(\omega)=g^2\int d\epsilon G_{HF}(\omega-\epsilon)D(\epsilon)f(\epsilon) \tag{21}$$

with $D(\epsilon)$ the bare phonon propagator again. This mean-field solution sums both the Hartree and Fock self-energy insertions to all orders, and would be identical to Migdal-Eliashberg theory if the dressed phonon propagator was employed in Eq. (21) rather than the bare propagator. As described in the Introduction, we are forced to use the bare propagator if we want to reproduce the IPT limit in the large-phonon-frequency limit. The Yosida-Yamada functional defined on G_{HF} is given by the diagrams in Fig. 2 where the solid lines are now Hartree-Fock propagators. The self-energy correction to G_0 for the HF expansion can then be written as

$$\Sigma(\omega)=\Sigma_{HF}+\Sigma_{YY}^{HF}[G_{HF}]. \tag{22}$$

The self-energy diagrams given in Figs. 1 and 2 are evaluated on the imaginary axis by using the standard rules [explicit expressions are given in Eq. (16) of Ref. 9 (and the suitable modifications for the Hartree-Fock case)] and the Matsubara summations occurring in $\Sigma_{YY}^{H}[G_H]$ and $\Sigma_{YY}^{HF}[G_{HF}]$ are performed numerically for both the Hartree and the Hartree-Fock expansions.

If the perturbative expansion for the self-energy is extended to higher order in U we find additional frequency-

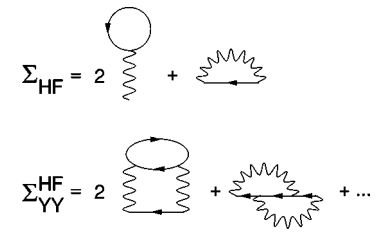

FIG. 2. Feynman diagrams included in the Hartree-Fock expansion. The top figure shows the Hartree and Fock diagrams, which are incorporated into G_{MF}, and the bottom shows the Yosida-Yamada functional about the Hartree-Fock mean-field solution expanded through second order. The wiggly lines are bare phonon propagators and the straight lines are Hartree-Fock (mean-field) propagators.

independent diagrams [which sum up to $U(n-n_{MF})$] in addition to the frequency-dependent diagrams (similar to the fifth diagram in Fig. 1). Here n is the fully renormalized particle number of the lattice that is calculated by Eq. (17) with G_{loc} replacing G_{MF}. These diagrams arise simply from the fact that in the exact skeleton expansion the Hartree diagram is evaluated with the fully dressed Green's function (yielding Un) rather than with the mean-field Green's function (which yields Un_{MF}). At half filling, the two fillings n and n_{MF} are usually equal, but they need not be the same (and never are) away from half filling. We introduce a new self-energy functional $\tilde{\Sigma}_{YY}^{H}[G_H]$ (that is based on the Yosida-Yamada functionals defined above) that has all of the higher-order renormalizations of the Hartree diagram removed from it [as shown, through third order in Fig. 3(a)]. Then we have an exact relation $\Sigma(\omega)=Un+\tilde{\Sigma}_{YY}^{H}[G_H]$ for the self-energy $\Sigma(\omega)$ defined in Eq. (14). In this contribution, the two self-energy functionals Σ_{YY}^{H} and $\tilde{\Sigma}_{YY}^{H}$ differ by one diagram (the fifth diagram in Fig. 1). We can employ this exact relation to formulate the renormalized-Hartree expansions[22] (also called the n-consistent approximation), which enforces this self-consistency condition on the renormalized particle number. That is, for a given μ, g, n_H, and

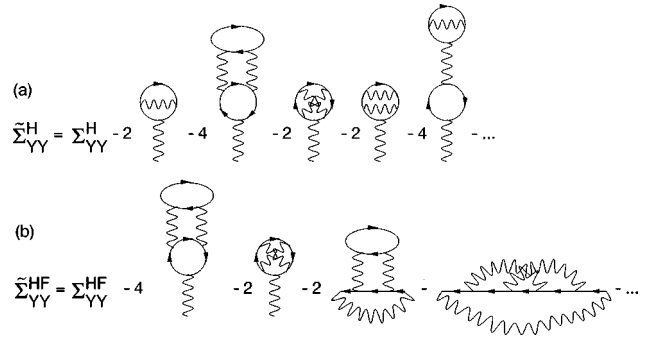

FIG. 3. Modified Yosida-Yamada functional for the renormalized expansions. (a) The renormalized-Hartree expansion (also known as the n-consistent approximation), in which all dressings of the Hartree diagram are removed from the Yosida-Yamada functional. (b) The renormalized Hartree-Fock expansion, in which all dressings of the Hartree and the Fock diagrams are removed from the Yosida-Yamada functional. The wiggly lines are the phonon propagators and the straight lines are the corresponding mean-field Green's functions (Hartree or Hartree-Fock).

$\tilde{\Sigma}^H_{YY}(\omega)$, we solve the transcendental equation,

$$n = -\frac{2}{\pi}\,\mathrm{Im}\sum_{\mathbf{p}}\int d\omega\,\frac{f(\omega)}{\omega-(\epsilon_{\mathbf{p}\sigma}-\mu)-Un-\tilde{\Sigma}^H_{YY}(\omega)}, \tag{23}$$

to determine the impurity electron filling n, and to obtain the correction to the real part of the total self-energy. For the Anderson and Wolff impurity models, and for the two-dimensional Hubbard model, this renormalized-Hartree approach (RH) expands the region of the validity of the perturbation theory and allows for the description of stronger correlations.[22,23] The hope is that this renormalized-Hartree scheme will repair some of the inaccuracies of the truncated perturbation theories away from half filling. It is a much simpler approximation to study than a scheme that tries to interpolate between the weak-coupling and atomic limits[24] (which is significantly more challenging to formulate for the electron-phonon problem).

A similar approach can be made for summing higher-order diagrams in the Hartree-Fock expansion. In this case, however, an n-consistent approximation, that sums only the frequency-independent diagrams to all orders, is likely to be less accurate than one that sums the renormalizations based on both the Hartree and Fock diagrams. Hence, we form the exact relation for the self-energy of Eq. (14),

$$\Sigma(\omega) = Un + g^2\int d\epsilon G_{loc}(\omega-\epsilon)D(\epsilon)f(\epsilon) + \tilde{\Sigma}^{HF}_{YY}[G_{HF}], \tag{24}$$

and employ it to evaluate the renormalized-Hartree-Fock expansion (RHF) where the functional $\tilde{\Sigma}^{HF}_{YY}(G_{HF})$ is truncated at second order [see Fig. 3(b)]. This approximation is formed by evaluating both the Hartree and Fock diagrams with the local Green's function (instead of G_{HF}) but the second-order diagrams continue to be evaluated with G_{HF}. In this sense it is ''halfway'' between a conserving approximation (which evaluates all diagrams with G_{loc}) and the truncated expansions described above.

The only remaining objects that need to be determined are the irreducible vertices for the CDW and SC instabilities. These vertices are calculated with the mean-field Green's function (either Hartree or Hartree-Fock) and have an identical functional form for all different approximation schemes. The diagrams included are presented in Fig. 4(a) for the CDW vertex and Fig. 4(b) for the SC vertex. The solid lines are G_{MF} (G_H or G_{HF}) and the wiggly lines are the bare phonon propagator. Explicit expressions for these diagrams on the imaginary axis are given in Eqs. (17) and (18) of Ref. 9 with G_0 replaced by G_{MF}.

III. CALCULATIONAL METHODS

The calculational methods used are straightforward. The perturbation expansion is carried out on the imaginary axis. We employ an iterational algorithm to solve the self-consistent equations, which is summarized in Fig. 5.

(1) Start with an initial self-energy $\Sigma(\omega)$.

(2) Use Eq. (12) to calculate G_{loc}.

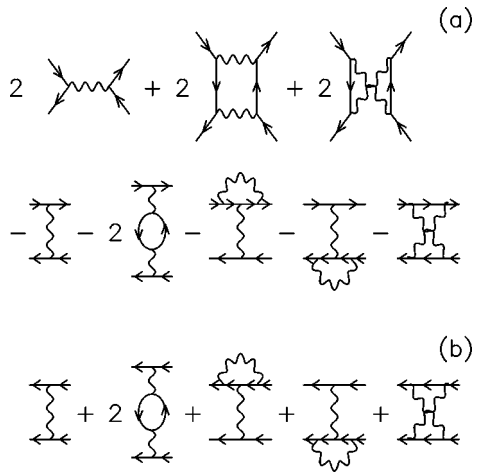

FIG. 4. Irreducible vertex functions for (a) charge-density-wave and (b) superconducting order. The wiggly lines are the bare phonon propagators and the straight lines are the corresponding mean-field propagators (Hartree or Hartree-Fock).

(3) Calculate the effective-medium propagator G_0 using Eq. (14) with $G_{imp}=G_{loc}$.

(4) Calculate the mean-field propagator using Eq. (16).

(5) Calculate the Yosida-Yamada self-energy diagrams as defined by Fig. 1 or Fig. 2, with and without the renormalization of the first-order diagrams (as shown in Fig. 3), to determine the total self-energy.

(6) If the calculation for the self-energy has not converged, then adjust the chemical potential to produce the target electron filling.

(7) Repeat steps (2)–(6) until the calculation has converged.

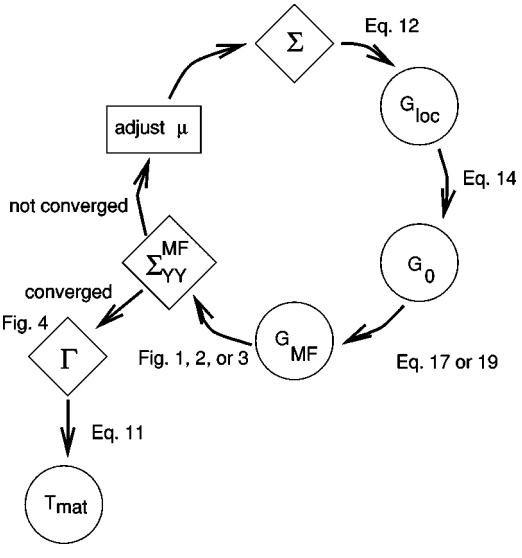

FIG. 5. Iterative algorithm for solving the self-consistent perturbation theory. As described in the text, one starts from an initial self-energy, then constructs the local Green's function, the effective-medium Green's function, and then the mean-field Green's function. The self-energy is then determined from the Yosida-Yamada expansion, and if the calculation is not converged, then the chemical potential is updated to adjust the electron filling and the process is repeated. If the calculation has converged, then the irreducible vertex functions are determined from Fig. 4, and the largest eigenvalue of the scattering matrix is then calculated.

(8) Once converged, calculate the irreducible vertex functions from Fig. 4 and determine the maximal eigenvalue of the scattering matrix in both the CDW and SC channels from Eq. (11).

(9) Repeat (1)–(8) for another temperature T until the transition temperature T_c is found.

We use an energy cutoff of 256 Matsubara frequencies, which provides accurate results for temperatures T larger than $0.01t^*$, and our convergence criterion is that the Green's functions do not change by more than one part in 10^9 from one iteration to the next. We find that the perturbation theory typically converges in approximately 100 iterations of the main ring in Fig. 5. Sometimes the iterated equations develop limit cycles, whose oscillations can be suppressed by employing standard damping methods that average the $(i-1)$st and ith iterations to produce the starting point for the next iteration. We also found that if the coupling strength is large enough, then some of the approximate theories will have multiple solutions for $n(\mu)$ near half filling. In this case, the symmetry point, with $\mu=U$, becomes unstable (i.e., the compressibility is negative), and the Green's functions are no longer purely imaginary when the electron filling is half filled. This latter result is an indication of the breakdown of the approximation method at such a large coupling strength.

There also are some technical details that need to be discussed about the quantum Monte Carlo simulations.[13] The results for the transition temperatures were calculated with a $\Delta\tau=0.4$, and sometimes also with a $\Delta\tau=0.2$ and then extrapolated to $\Delta\tau=0$ when the correlations were large enough that the Trotter error was noticeable. The self-energies and irreducible vertex functions were calculated with a fixed $\Delta\tau=0.1$ to ensure a high accuracy. In general, there are three sources of error to the quantum Monte Carlo simulation: (i) statistical error; (ii) iteration error; and (iii) systematic error. The statistical error is the easiest error to control, and is the smallest of the three sources of error. The iteration error arises from performing calculations with the wrong dynamical mean field G_0 because the calculation has not yet converged fully. We typically iterate 8 or 9 times, which provides good convergence for the iterations. The systematic error is more difficult to control. It arises from the Trotter error, and from other (potentially unknown) sources. One surprising source of error arose from the choice of global updating moves for the phonon coordinate. Global moves that shift the phonon coordinate at every time slice by an amount randomly chosen between $-dx/2$ and $dx/2$ were supplemented by global shifts by an amount ranging between $\pm 2g/(m\Omega^2)-dx/2$ and $\pm 2g/(m\Omega^2)+dx/2$. These latter moves were chosen to allow the phonon coordinate to shift between the two minima of the effective phonon potential (separated by $2g/[m\Omega^2]$), which form when the system enters the strong-coupling region, where preformed pairs exist above T_c. When one is in the weak-coupling regime, where the effective phonon potential possesses a single-well structure, we find that the self-energy can differ by a few percent depending on whether the global moves are all chosen randomly, or if the supplemental global shifts are chosen to move the phonon coordinate to the ''other'' well (i.e., if the phonon coordinates lie in the right well then the global shift is chosen to move the system to the left, and vice versa). The accuracy was best when the global moves were chosen completely randomly, which is the method used here. These results differ by a few percent from those shown previously,[9] where the global moves were coupled to the values of the phonon coordinates, and the Trotter time slice was larger.

IV. RESULTS AND DISCUSSION

The parameters of the Hamiltonian in Eq. (1) are chosen to agree with previous theoretical work, and to represent a parameter range where the vertex corrections can cause large effects. As such, we choose the phonon frequency to be on the order of one-tenth of the bandwidth $\Omega=0.5t^*$ (with the effective bandwidth of the Gaussian being about two standard deviations above and below the center, or approximately $4t^*$). Most of our calculations are performed for three different values of the interaction strength: (i) $g=0.4$ ($U=-0.64$, one-sixth of the bandwidth), which corresponds to a fairly weak interaction where there are no preformed pairs, but the transition temperatures are large enough that the phase diagram can be determined reliably; (ii) $g=0.5$ ($U=-1.0$, one-fourth of the bandwidth), which is in the moderate interaction regime; and (iii) $g=0.625$ ($U=-1.5625$, two-fifths of the bandwidth), which is where the system enters the strongly coupled regime, where numerous preformed pairs are present above T_c.

The quasiparticle renormalization factor, the irreducible CDW vertex function, and the irreducible SC vertex function are plotted in Figs. 6(a)–6(c). The vertex functions are averaged to show just the symmetric frequency component, since that is all that contributes to the eigenvalue of the scattering matrix for the CDW at half filling, or for the SC at any filling (this is so because the eigenvector with maximal eigenvalue is symmetric with respect to a change in sign of the Matsubara frequency). The coupling strength is $g=0.4$ and the filling is $n=1.0$, which yields a bare electron-phonon coupling strength of $|U|=0.64$, or $\lambda=\rho(0)|U|=0.36$, which would naively be viewed as quite weak coupling. However, this is not the case, as one can estimate the renormalized value of λ from $Z(0)-1$ which lies at about 0.7. These calculations indicate that higher-order diagrams, such as those that fully dress the phonon propagator, are important even when the bare coupling has $\lambda=0.36$. What is interesting is that the perturbative results seem to have the right shape, but need to have the frequency axis moved to the right to line up with the Monte Carlo data. Furthermore, since the perturbation theory underestimates both the renormalization factor (which will enhance T_c) and the vertex function (which will reduce T_c) one might expect these results to tend to cancel each other out when calculating a phase diagram, which is indeed what we find below. Figures 7(a)–7(c) show the same results for the stronger coupling case $g=0.5$ and $n=1.0$ ($|U|=1.0$ and $\lambda=0.56$). We can see that the error in the renormalization factor has grown, even though all four perturbative methods yield similar values. The CDW vertex becomes more attractive at moderate coupling, which is missed by the perturbation theory. The SC vertex has the right qualitative shape, but is underestimated at low frequencies. When the coupling strength is increased to $g=0.625$ (not shown) the situation becomes even worse, with the same qualitative features seen, a growing difference in the renormalization fac-

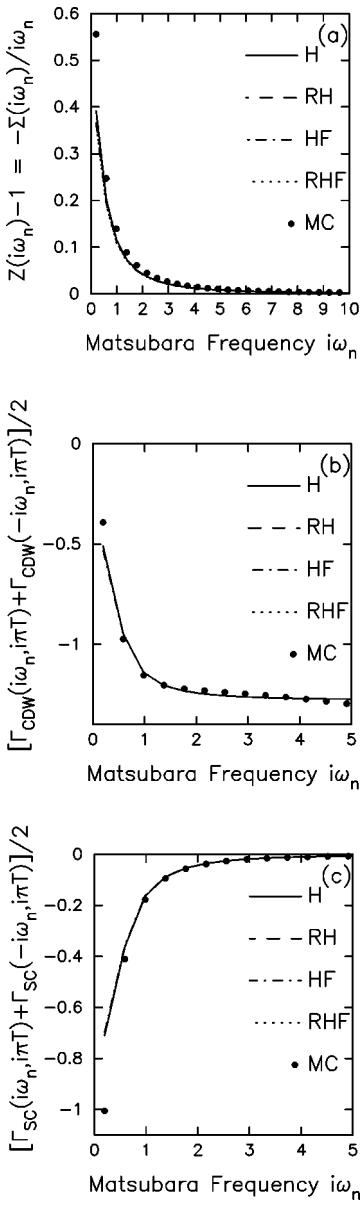

FIG. 6. Self-energy and irreducible vertex functions for the Holstein model at half filling ($n=1.0$) and weak coupling $g=0.4$. The temperature is just above T_c at $T=1/16$. (a) shows the quasiparticle renormalization factor minus 1 as a function of frequency. The four different expansion schemes (Hartree, renormalized Hartree, Hartree-Fock, and renormalized Hartree-Fock) are plotted with lines, and the quantum Monte Carlo is plotted with solid dots. We believe the combined errors on the simulation to be on the order of a few percent. (b) is the CDW vertex and (c) is the SC vertex.

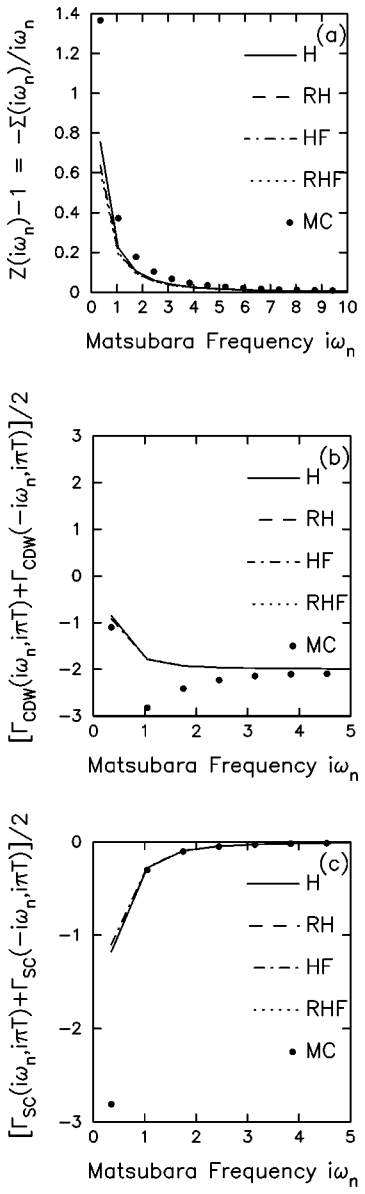

FIG. 7. Self-energy and irreducible vertex functions for the Holstein model at half filling ($n=1.0$) and moderate coupling $g=0.5$. The temperature is just above T_c at $T=1/9$. (a), (b), and (c) are the quasiparticle renormalization factor minus 1, the CDW vertex, and the SC vertex, respectively. Note how the agreement with the perturbation theory worsens as the coupling strength is increased.

tors, and an underestimation of the size of the vertices.

We also include, in Fig. 8, a result at quarter filling $n=0.5$ and $g=0.4$ at the same temperature $T=1/16$ as in Fig. 6. One might have thought that the quarter-filled case would be approximated much better by the perturbation theory because the effective coupling strength is lower due to the reduction of the electronic density of states at the Fermi level, but we see that the shape of the curves is both qualitatively and quantitatively similar for Figs. 6 and 8. The quantitative agreement has improved, but the improvement is not dramatic. What is surprising is that the calculated transition temperature agrees much better with the QMC here than at half filling, because of the cancellation of the errors to both the self-energy and the vertex function. Note that we only plot the SC vertex here, because an asymmetric average is needed for the physically relevant piece of the CDW vertex.

In addition to calculating the single-particle and two-particle self-energies, we can also investigate the phase diagrams of the Holstein model. Based on our results for the self-energy and the vertex functions, it does not appear likely that any approximation will be too accurate for the phase diagrams, but as theorized above, it is possible that the inaccuracies will cancel out to produce more accurate results for the transition temperatures. Such behavior should be viewed as ''accidental'' agreement with the exact result.

We begin by calculating the transition temperature to the

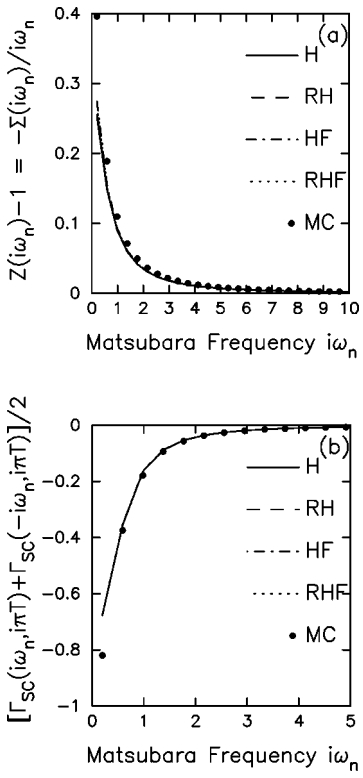

FIG. 8. Self-energy and irreducible vertex functions for the Holstein model at quarter filling ($n=0.5$) and weak coupling $g=0.4$. The temperature is the same as in Fig. 6, $T=1/16$. (a) is the quasiparticle renormalization factor minus 1 and (b) is the SC vertex. Note how the perturbation theory has improved, but less than what would have been expected naively.

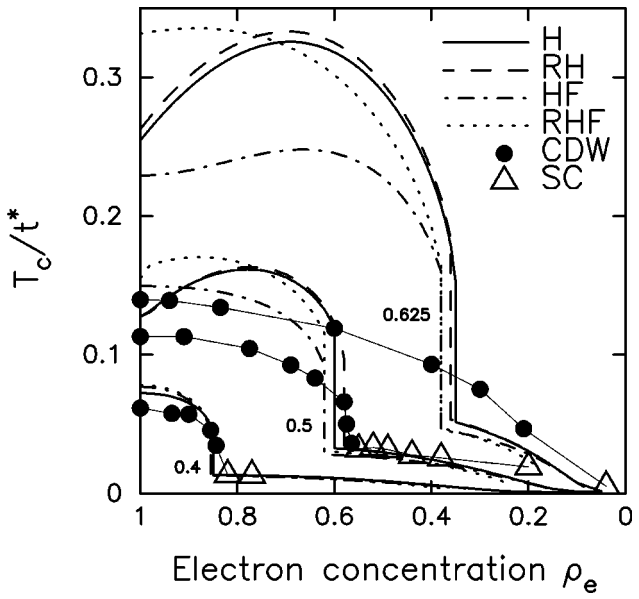

FIG. 10. Phase diagram of the Holstein model away from half filling for three different coupling strengths $g=0.4$, $g=0.5$, and $g=0.625$. The lines through the QMC data points are guides to the eye. Note that the SC transition temperatures are approximated better than the CDW transition temperatures, and that the phase diagrams are predicted more accurately than would be expected from the individual self-energies or vertex functions. As the coupling strength is increased the T_c's are all enhanced significantly, and the location of the CDW-SC phase boundary is predicted less accurately. The renormalized expansions do sometimes improve the qualitative shape of the phase boundaries to show a maximum T_c at half filling, but the perturbative approach is definitely breaking down as the coupling strength becomes larger than 0.5.

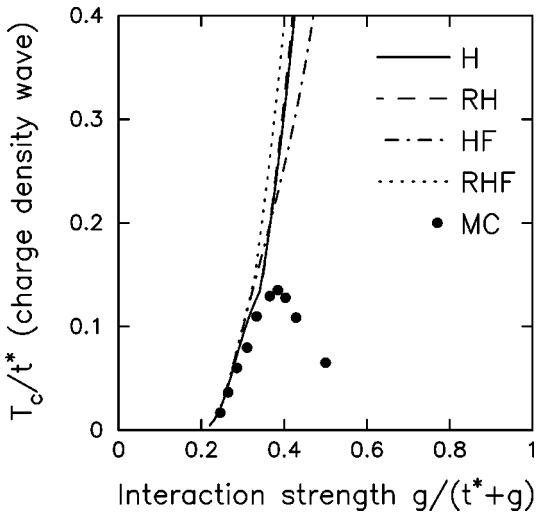

FIG. 9. Phase diagram of the Holstein model at half filling. The four different expansion schemes (lines) are compared to the quantum Monte Carlo (dots). Note how all perturbative approximations do not show a peak in the CDW transition temperature at half filling, but rather continue to increase. The Hartree and renormalized Hartree expansions are identical until the solution at half filling (with chemical potential $\mu=U$) becomes unstable for the RH expansion, and the Green's functions acquire real parts.

commensurate (checkerboard) CDW insulator at half filling as a function of the interaction strength. The QMC solution[13] showed that the maximal T_c was on the order of 1/25th of the bandwidth, occurring when U was about two-fifths of the bandwidth. The results for each of the four expansions shown here is presented in Fig. 9. The horizontal axis is the interaction strength and the vertical axis is the transition temperature. One can see that the peak in T_c versus U is not produced by the perturbation theory, rather the transition temperature continues to increase. This differs from what happened in the so-called IPT approximation where the approximate curve for T_c did show a peak.[9] The Hartree and renormalized-Hartree expansions agree with each other and the IPT approximation until U is approximately -1, where they differ from each other because the thermodynamically stable H and RH expansions are no longer at the particle-hole symmetric point with $\mu=U$, but rather have different values of μ (and no longer have purely imaginary Green's functions when evaluated along the imaginary axis). This is the point where the kink appears in the $T_c(g)$ curve. The remarkable agreement of the IPT approximation in predicting both the peak position and the peak height accurately is really just a coincidence, since neither the self-energy nor the vertex function is reproduced well at that value of the interaction strength (see Figs. 6–8). There is a very delicate balance between the self-energy terms (which tend to reduce T_c as the interaction increases) and the vertex-function terms (which tend to increase T_c as the interaction increases) that

causes T_c to have a peak for the IPT approximation, but continue to increase for the approximations in this contribution.

We end with a calculation of the phase diagrams off of half filling, which show the transition from the checkerboard CDW insulator to a SC. These results are plotted in Fig. 10. The horizontal axis is the electron filling and the vertical axis is the transition temperature to either a CDW or SC phase. The CDW-SC phase boundary lies at the points where the phase diagrams have a slope discontinuity. Three values of interaction strength are included, and both the approximate solutions and the QMC results are presented (the lines through the QMC data are just a guide to the eye). The agreement for T_c is quite good for the weak-coupling value $g=0.4$, with all approximations going through the QMC data for the SC phase, and overestimating T_c only slightly for the CDW phase. Here, the Hartree-Fock expansion is actually worse than the Hartree expansion for the CDW phase. The calculation also seems to underestimate the location of the CDW-SC phase boundary. The case with $g=0.5$ begins to show how the solutions develop qualitatively wrong behavior near half filling. All but the Hartree-Fock expansion show a suppression of T_c as the filling approaches 1. Such a suppression was never seen in the QMC simulations, and is likely an artifact of the nonconserving nature of the approximations.[9] It continues to be clear that the SC solutions are approximated better than the CDW solutions, and that the approximations behave worst near half filling. In particular, it is important to note that the simple n-consistent scheme, which worked so well for the Hubbard model, does not appear to work as well for the electron-phonon problem examined here because the phase diagrams (H and RH) continue to have qualitatively incorrect behavior. Finally we examine the strongly coupled case $g=0.625$. Here the renormalized expansions do a better job at repairing the qualitatively wrong behavior of a T_c suppression near half filling, but they do so by greatly enhancing the T_c's at and near half filling from the truncated expansions. It is clear that at this large a value of the coupling strength none of these weak-coupling approaches is doing a good job at predicting the phase diagrams. It is interesting to note that the close agreement of the Hartree and renormalized-Hartree calculations shows that the majority of the shift of the chemical potential comes from the Fock dressing of the Hartree diagram. Surprisingly, the inclusion of this diagram has a large effect on the phase diagram when $|U|>1$.

V. CONCLUSIONS

What are the conclusions that can be drawn from this work? Even at a weak value of the bare interaction strength ($g=0.4$) both the self-energy and the irreducible vertex functions are not approximated accurately by the perturbation theory. This implies that third-order (and higher-order) diagrams are important and cannot be neglected. For example, it is possible that a scheme that uses an expansion with dressed phonon propagators would be more accurate, which is work in progress. Nevertheless, the perturbation theory does appear to produce a more accurate approximation to the phase diagrams than the individual self-energies. On the other hand, these results show that there is no simple scheme that will allow one to approximate the electron-phonon problem accurately for all values of the phonon frequency. So one should not necessarily rely on approximations that employ purely electronic models (such as the Hubbard model) to carry over to the electron-phonon problem and work well when the phonon frequency is small to moderate. Instead, it is more fruitful to work on generalizations of the Migdal-Eliashberg theory that work with dressed phonons, but include higher-order nonadiabatic effects such as vertex corrections. This should save a lot of time in formulating accurate approximation methods for real materials that have large enough phonon energy scales that the effects of nonconstant density of states and of vertex corrections cannot be neglected. Working with dressed phonons actually makes a lot of sense for the electron-phonon problem, because experiments can directly measure the dressed phonon spectral function, so it is readily available for use in real materials calculations. Furthermore, the dressed phonon propagator can be extracted from the QMC simulation and used in the perturbation theory for the electrons, just as is done from experiments on real materials. Work along these lines is currently in progress.

ACKNOWLEDGMENTS

We would like to thank Paul Miller and Joe Serene for useful discussions. J.K.F. and W.C. acknowledge support for the initial stages of this work from the Office of Naval Research Young Investigator Program N000149610828 and J.K.F. and V.Z. acknowledge support for the final stages of this work from the National Science Foundation INT-9722782 and DMR-9627778. M.J. acknowledges support from the National Science Foundation DMR-9704021 and DMR-9357199, and from the Ohio Supercomputer Center.

[1] J. Bardeen, L. Cooper, and J. Schrieffer, Phys. Rev. **108**, 1175 (1957).

[2] A. B. Migdal, Zh. Eksp. Teor. Fiz. **34**, 1438 (1958) [Sov. Phys. JETP **7**, 999 (1958)].

[3] G. M. Eliashberg, Zh. Eksp. Teor. Fiz. **38**, 966 (1960) [Sov. Phys. JETP **11**, 696 (1960)].

[4] *Superconductivity*, edited by R. Parks (Dekker, New York, 1969).

[5] P. B. Allen and R. C. Dynes, Phys. Rev. B **12**, 905 (1975); P. B. Allen and B. Mitrović, Solid State Phys. **37**, 1 (1982); J. P. Carbotte, Rev. Mod. Phys. **62**, 1027 (1990); H.-S. Wu, Z.-Y Weng, G. Ji, and Z.-F. Zhou, J. Phys. Chem. Solids **48**, 395 (1987).

[6] T. Holstein, Ann. Phys. (N.Y.) **8**, 325 (1959).

[7] J. Hubbard, Proc. R. Soc. London, Ser. A **276**, 238 (1963).

[8] A. Georges and G. Kotliar, Phys. Rev. B **45**, 6479 (1992).

[9] J. K. Freericks and M. Jarrell, Phys. Rev. B **50**, 6939 (1994).

[10] W. Metzner and D. Vollhardt, Phys. Rev. Lett. **62**, 324 (1989).

[11] H. Schweitzer and G. Czycholl, Z. Phys. B **77**, 327 (1990).

[12] W. Metzner, Phys. Rev. B **43**, 8549 (1991).

[13] J. E. Hirsch and R. M. Fye, Phys. Rev. Lett. **56**, 2521 (1986); M.

Jarrell, *ibid.* **69**, 168 (1992); M. Jarrell and Th. Pruschke, Z. Phys. B **90**, 187 (1993); Th. Pruschke, D. L. Cox, and M. Jarrell, Phys. Rev. B **47**, 3553 (1993); J. K. Freericks, M. Jarrell, and D. J. Scalapino, *ibid.* **48**, 6302 (1993); Europhys. Lett. **25**, 37 (1994); J. K. Freericks and M. Jarrell, in *Computer Simulations in Condensed Matter Physics*, edited by D. P. Landau, K. K. Mon, and H.-B. Schüttler (Springer-Verlag, Heidelberg, 1994), Vol. VII.

[14] V. Zlatić and B. Horvatić, Solid State Commun. **75**, 263 (1990).

[15] U. Brandt and C. Mielsch, Z. Phys. B **75**, 365 (1989).

[16] E. Müller-Hartmann, Z. Phys. B **74**, 507 (1989); **76**, 211 (1989); B. Menge and E. Müller-Hartmann, *ibid.* **82**, 237 (1991).

[17] C. S. Owen and D. J. Scalapino, Physica (Utrecht) **55**, 691 (1971).

[18] P. W. Wolff, Phys. Rev. **124**, 1030 (1961); H. R. Krishnamurty, J. W. Wilkins, and K. G. Wilson, Phys. Rev. B **21**, 1003 (1980).

[19] G. Baym and L. P. Kadanoff, Phys. Rev. **124**, 287 (1961); G. Baym, *ibid.* **127**, 1391 (1962); N. E. Bickers and D. J. Scalapino, Ann. Phys. (N.Y.) **193**, 206 (1989).

[20] K. Yosida and K. Yamada, Prog. Theor. Phys. **46**, 244 (1970); K. Yamada, *ibid.* **53**, 970 (1975); K. Yosida and K. Yamada, *ibid.* **53**, 1286 (1975); K. Yamada, *ibid.* **54**, 316 (1975); **55**, 1345 (1976); **62**, 354 (1979).

[21] V. Zlatić and B. Horvatić, Phys. Rev. B **40**, 3368 (1989).

[22] B. Horvatić and V. Zlatić, Solid State Commun. **54**, 957 (1985).

[23] V. Zlatić (unpublished).

[24] H. Kajueter and G. Kotliar, Phys. Rev. Lett. **77**, 131 (1996).